Journal Pre-proofs

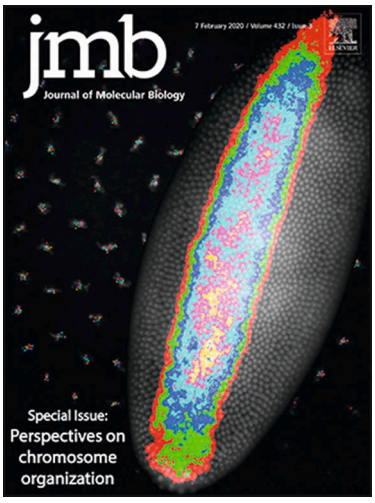

Research Article

The specific elongation factor to selenocysteine incorporation in Escherichia coli: unique tRNA^{Sec} recognition and its interactions

Vitor Hugo Balasco Serrão, Adriano de Freitas Fernandes, Luis Guilherme Mansor Basso, Jéssica Fernandes Scortecci, Edson Crusca Júnior, Marinônio Lopes Cornélio, Bibiana Monson de Souza, Mário Sérgio Palma, Mario de Oliveira Neto, Otavio Henrique Thiemann

PII: S0022-2836(21)00516-7
DOI: https://doi.org/10.1016/j.jmb.2021.167279
Reference: YJMBI 167279

To appear in: *Journal of Molecular Biology*

Received Date: 30 June 2021
Revised Date: 22 September 2021
Accepted Date: 23 September 2021

Please cite this article as: V. Hugo Balasco Serrão, A. de Freitas Fernandes, L. Guilherme Mansor Basso, J. Fernandes Scortecci, E. Crusca Júnior, M. Lopes Cornélio, B. Monson de Souza, M. Sérgio Palma, M. de Oliveira Neto, O. Henrique Thiemann, The specific elongation factor to selenocysteine incorporation in Escherichia coli: unique tRNA^{Sec} recognition and its interactions, *Journal of Molecular Biology* (2021), doi: https://doi.org/10.1016/j.jmb.2021.167279

The specific elongation factor to selenocysteine incorporation in Escherichia coli: unique tRNA^{Sec} recognition and its interactions

Vitor Hugo Balasco Serrão[a,b†]; Adriano de Freitas Fernandes[a†]; Luis Guilherme Mansor Basso[c,d]; Jéssica Fernandes Scortecci[a,e]; Edson Crusca Júnior[f]; Marinônio Lopes Cornélio[g]; Bibiana Monson de Souza[h]; Mário Sérgio Palma[h]; Mario de Oliveira Neto[i] and Otavio Henrique Thiemann[a,j*]

[a] Physics Institute of Sao Carlos, University of Sao Paulo. Trabalhador Sao Carlense Av., 400. São Carlos, SP, CEP 13566-590, Brazil;
[b] Department of Chemistry and Biochemistry, University California – Santa Cruz. 1156 High St., Santa Cruz, CA, 95060, United States;
[c] Physical Sciences Laboratory, State University of Northern Rio de Janeiro Darcy Ribeiro – UENF, Av. Alberto Lamego, 2000, 28013-602, Campos dos Goytacazes, RJ, Brazil;
[d] Faculty of Science, Philosophy and Letters, University of Sao Paulo, CEP 14040-901, Ribeirão Preto, SP, Brazil;
[e] Department of Biochemistry and Molecular Biology, University of British Columbia. 2350 Health Science Mall, Vancouver, British Columbia, V6T 1Z3, Canada;
[f] Department of Physical Chemistry, Chemistry Institute of the São Paulo State University – UNESP, CEP 14800-900, Araraquara, SP, Brazil;
[g] Physics Department, Institute of Biosciences, Letters and Exact Sciences (IBILCE), São Paulo State University – UNESP, São Jose do Rio Preto, SP, Brazil;
[h] Department of General and Applied Biology, Institute of Biosciences of Rio Claro, São Paulo State University – UNESP, Rio Claro, SP, Brazil;
[i] Bioscience Institute of Universidade Estadual Paulista. Rubião Jr., Botucatu, SP, CEP 18618-000, Brazil;
[j] Department of Genetics and Evolution, Federal University of São Carlos – UFSCar, 13565-905 São Carlos, SP, Brazil.

[†] Both authors contributed equally to this work.
* Corresponding author: thiemann@ifsc.usp.br

Present address: 1100 Joao Dagnone Av, Jardim Santa Angelina – Sao Carlos, SP – Brazil. Physics and Informatics Department, Physics Institute of Sao Carlos, University of Sao Paulo – USP, CEP 13563-120 Sao Carlos, SP - Brazil. +55 16 3373 8089. thiemann@ifsc.usp.br

ABSTRACT

Several molecular mechanisms are involved in the genetic code interpretation during translation, as codon degeneration for the incorporation of rare amino acids. One mechanism that stands out is selenocysteine (Sec), which requires a specific biosynthesis and incorporation pathway. In *Bacteria,* the Sec biosynthesis pathway has unique features compared with the eukaryote pathway as Ser to Sec conversion mechanism is accomplished by a homodecameric enzyme (selenocysteine synthase, SelA) followed by the action of an elongation factor (SelB) responsible for delivering the mature Sec-tRNA^{Sec} into the ribosome by the interaction with the Selenocysteine Insertion Sequence (SECIS). Besides this mechanism being already described, the sequential events for Sec-tRNA^{Sec} and SECIS specific recognition remain unclear. In this study, we determined the order of events of the interactions between the proteins and RNAs involved in Sec incorporation. Dissociation constants between SelB and the native as well as unacylated-tRNA^{Sec} variants demonstrated that the acceptor stem and variable arm are essential for SelB recognition. Moreover, our data support the sequence of molecular events where GTP-activated SelB strongly interacts with SelA.tRNA^{Sec}. Subsequently, SelB.GTP.tRNA^{Sec} recognizes the mRNA SECIS to deliver the tRNA^{Sec} to the ribosome. SelB in complex with its specific RNAs were examined using Hydrogen/Deuterium exchange mapping that allowed the determination of the molecular envelopes and its secondary structural variations during the complex assembly. Our results demonstrate the ordering of events in Sec incorporation and contribute to the full comprehension of the tRNA^{Sec} role in the Sec amino acid biosynthesis, as well as extending the knowledge of synthetic biology and the expansion of the genetic code.

HIGHLIGHTS

- Elucidate the Sec incorporation pathway having SelB as checkpoint through the dissociation constant values observed in the formation of complexes with tRNA, SECIS element, SelA, and ribosome
- Determine the order of events in the withdrawal process of tRNA^{Sec} from binary complex SelA.tRNA^{Sec} and delivery to the ribosome
- Low-resolution mapping of SelB and its complexes with tRNA^{Sec} and SECIS element

GRAPHICAL ABSTRACT

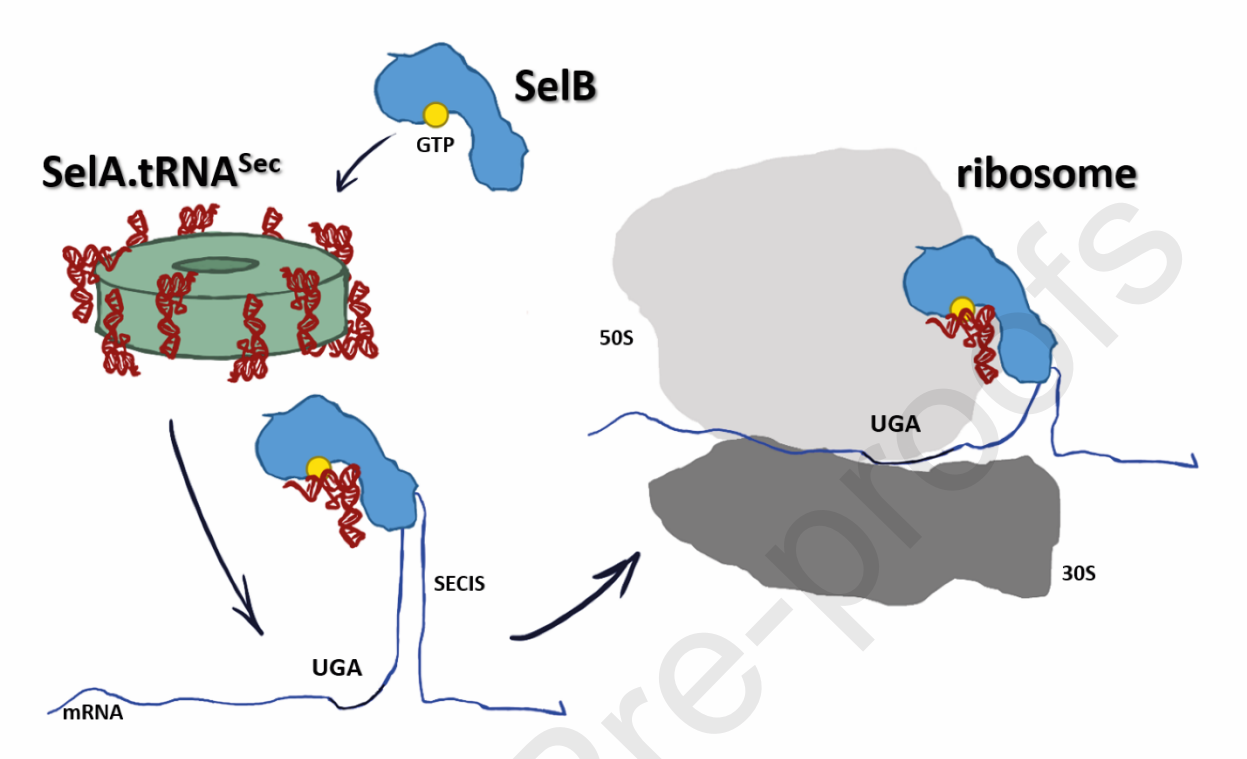

KEYWORDS:

selenocysteine; elongation factor; SelB; tRNA[Ser]Sec, protein-RNA interaction.

ABBREVIATIONS

EFs: Elongation Factors; Sec: Selenocysteine; SelC or tRNA[Ser]Sec: specific unacylated-RNA transporter for Sec incorporation; Ser: Serine; SerRS: Seryl-tRNA synthetase; PLP: Pyridoxal 5'-phosphate; SelA: Selenocysteine synthase; SECIS: SelenoCysteine Insertion Sequence; SelB: selenocysteine-specific elongation factor; WHD: *winged helix domain*; SDS-PAGE: sodium dodecyl sulphate-polyacrylamide gel electrophoresis; HPLC: High-Performance Liquid Chromatography; FA: fluorescence anisotropy assays; K_D: apparent dissociation constant; AUC: analytical ultracentrifugation; DSC: differential scanning calorimetry; FTIR: *Fourier* Transform Infrared spectroscopy; HDx: Hydrogen/Deuterium exchange; SAXS: small angle X-ray scattering; IPTG: isopropyl β-D-1-thiogalactopyranoside; SEC: Size-exclusion chromatography; EDTA: ethylenediaminetetraacetic acid; ACN: acetonitrile.

INTRODUCTION

Elongation factors (EFs) are responsible for the delivery of amino acid carrying tRNAs to the ribosomal machinery for its nascent peptide incorporation [1,2]. Usually, different amino acids are recognized by the same EF. However, selenocysteine (Sec, U), one of the rare amino acids, is specifically recognized by a unique EF named, in *Bacteria*, as SelB [3–5].

Sec is co-translationally incorporated into selenoproteins involved in several functions such as oxidoreduction, redox signaling, and antioxidant defense [3,6–8]. The synthesis of Sec is peculiar among the amino acids because it takes place on a specific tRNA ($tRNA^{Sec}$ or SelC) charged with L-serine (Ser). Ser is converted to Sec by selenocysteine-specific biosynthesis machinery [9–12]. Briefly, the Sec biosynthesis in *Bacteria* starts with the specific aminoacylation of the $tRNA^{[Ser]Sec}$ with a Ser residue by seryl-tRNA synthetase (SerRS, E.C. 6.1.1.1), forming the Ser-$tRNA^{[Ser]Sec}$ [13]. The charged $tRNA^{[Ser]Sec}$ is the substrate for the homodecameric PLP-dependent enzyme selenocysteine synthase (SelA, E.C. 2.9.1.1) responsible for Ser to Sec conversion resulting in the mature Sec-$tRNA^{Sec}$ [14–17]. The incorporation of Sec into selenoproteins is directed at a UGA-Stop codon, misinterpreted as a UGA-Sec codon, by the presence of a specific mRNA structure called Selenocysteine Insertion Sequence (SECIS) [18,19]. Sec-$tRNA^{Sec}$ is recognized by a selenocysteine-specific elongation factor (SelB, E.C. 3.6.5.-), which is responsible for capturing the charged tRNA and delivering it to the translational machinery for incorporation into selenoproteins, avoiding the release factor for the UGA-codon recognition [4,20–25].

SelB has an N-terminal GTPase domain similar to canonical EFs, with a unique *winged-helix domain* (WHD) responsible for the recognition of the "8+5" $tRNA^{Sec}$ conformation. A long C-terminal domain is responsible for the interaction and binding with the SECIS sequence [22,23,26–29], providing the specificity to UGA-Sec codon identification [30–32]. Previous studies provided a snapshot view of the Sec incorporation process, revealing that the SelB.GTP.Sec-$tRNA^{Sec}$ complex is stabilized by the interaction with the SECIS-ribosome complex, delivering the Sec-$tRNA^{Sec}$ to the ribosome A site [31,33]. However, the specific sequential mechanism of Sec-$tRNA^{Sec}$ and SECIS recognition is not yet fully characterized.

In this report, we characterized the selectivity and specificity of *Escherichia coli* SelB interaction with unacylated-$tRNA^{Sec}$ and six different unacylated-$tRNA^{Sec}$ variants, showing the tRNA structural motifs involved in SelB recognition. Subsequently, we also demonstrated the SelB.tRNA complex interaction with selenocysteine synthase (*Ec*SelA). The bacterial Sec-synthesis complex interaction with the ribosome has also been investigated, using a specific Sec-insertion sequence

from bacterial formate dehydrogenase-H (FDH-H). These results revealed the sequence of events in the formation of these complexes for Sec delivery. Furthermore, our molecular models reveal the conformational changes occurring during the complex's formation. Our model explains the Sec incorporation into selenoproteins as well as elucidates the importance of tRNA structural elements for this specific biosynthesis pathway.

RESULTS

SelB, nucleic acid, and nucleotide-free sample purification

Purified bacterial SelB was obtained by sequential affinity and size exclusion chromatography purifications, revealing a monodisperse population with a molecular weight of approximately 70 kDa, as expected for a monomer in solution, and absence of contaminants as monitored by SDS-PAGE and western-blot (**Supplementary Figure 1**). Moreover, the purified SelB was sequenced by mass spectrometry, with 52% sequence coverage. Similar to most of the elongation factors, SelB is an RNA/GTP-binding protein. Therefore, the presence of endogenous RNA/GTP is expected during the purification process, which affects the measurement of interaction constants. The absence of endogenous GTP/GDP nucleotides co-purified with recombinant SelB was monitored by High-Performance Liquid Chromatography (HPLC) after treatment with RNAse A (**Supplementary Figure 2**). As previously described, SelB presents high dissociation constant (K_D) values for GTP and GDP as 0.74 and 12 μM, respectively [26]. Due to this low affinity using *in vitro* conditions, purified SelB does not contain co-purified endogenous nucleotides, therefore revealing the GTP-addition dependence for the binding assays.

tRNA^{Sec} structural elements importance in SelB binding

SelB specifically recognizes and interacts with two different nucleic acid elements, the Sec-tRNA$^{Ser[Sec]}$ and the SECIS element. Five unacylated-tRNA^{Sec} variants were generated by replacing its structural elements (acceptor, anticodon, D-loop, TψC, and variable stems) with the corresponding tRNA^{Ser} (GGA) and a variable arm deleted tRNA^{Sec} form [34].

The specific interaction between SelB and tRNA^{Sec} was monitored by fluorescence anisotropy assays (FA) using covalently labeled fluorescein-5-maleimide tRNA^{Sec}, its variants, and unacylated-tRNA^{Ala} as a negative control. Labeled tRNAs were maintained constant whereas increasing concentrations of SelB were sequentially added, obtaining the binding profile (**Figure 1**) summarized in **Table 1**.

SelB.GTP.tRNA^{Sec} complex formation resulted in a K_D of (283 ± 53) nM, as expected for this molecular complexation [26]. The anticodon and D-loop variants do not affect tRNA^{Sec} binding to SelB.GTP, resulting in K_D values of (269 ± 29) nM and (285 ± 42) nM, respectively, similar to the wild-type tRNA^{Sec}. These observed values are similar to those obtained by Paleskava *et al*. [26] also Dell and Johnson [35].

The unacylated-tRNA^{Sec} clearly affects the interactions, resulting in a drastic increase in the apparent K_D in comparison with the acylated-tRNA^{Sec} affinity in presence of GTP – (0.21 ± 0.06) pM [36]. However, previous reports have extensively demonstrated the usage of unacylated-tRNA^{Sec} is considered valid to determine the binding constants since the key structural elements for its recognition are preserved in the tRNA folding [16,17,34].

Moreover, variations on acceptor stem, TψC-loop, and variable arm (deletion – tRNA$^{Sec}_{\Delta Var}$ - or replacement for tRNA$^{Ser}_{Var}$) resulted in K_D values of (584 ± 89) nM, (501 ± 69) nM, (721 ± 90) nM and (491 ± 44) nM, respectively. These values are similar to unacylated-tRNA^{Ala} (646 ± 129) nM, used as a negative control for SelB specificity and corroborate previous structural information [30,31].

The SelB.GTP.tRNA^{Sec} complex formation using tRNA^{Sec} variants was also determined by sedimentation velocity analytical ultracentrifugation (**Supplementary Figure 3**). The sedimentation coefficients (**Table 2**) revealed that SelB.GTP sediment as a single species of (4.779 S) while the binary complex (SelB.GTP.tRNA^{Sec}) prepared with excess SelB, show an additional peak (7.310 S). The higher sedimentation coefficients observed for the tRNA^{Sec} variants denote the increase in the complex shape. In other words, the complexes are not assembled in a compact conformation in comparison with SelB.GTP.tRNA^{Sec} but less flexible than SelB in complex with tRNA^{Ala}, as shown by the hydrodynamic (*Stokes*) radii (**Table 2**). Interestingly, the complex does not form with the variable arm deleted tRNA^{Sec} (tRNA$^{Sec}_{\Delta Var}$).

Moreover, sedimentation equilibrium analytical ultracentrifugation was used to investigate the effect of the variable arm in the SelB.GTP.tRNA^{Sec} complex formation (**Supplementary Figure 4** and **Table 3**). The K_D values reveal that the variable arm is critical for SelB.GTP.tRNA^{Sec} interaction, which was also observed by higher K_D values observed by fluorescence anisotropy.

Macromolecular interactions during Sec biosynthesis and incorporation pathway

The formation of SelB.GTP.SECIS.tRNA^{Sec} quaternary complex was analyzed using *in vitro* transcribed fluorescein-labeled SECIS from *E. coli* formate dehydrogenase (FDH-H), and tRNA^{Sec}. The SelB.GTP.SECIS dissociation constant of (57 ± 13) nM and cooperativity factor of (2.6 ± 1.5) indicates a specific binding of SelB.GTP to the SECIS with high affinity and cooperatively favorable (**Figure 2a** and **Table 4**). Analysis of the SelB.GTP.SECIS.tRNA^{Sec} quaternary complex formation revealed a K_D value of (895 ± 57) nM (**Figure 2b**), where the previously formed SelB.GTP.SECIS complex was titrated against fluorescein-labeled tRNA^{Sec}. However, a similar interaction was not observed in the equivalent experiment of SelB.GTP.tRNA^{Sec} binding to labeled SECIS. The observed affinity of (77 ± 3) nM for the formation of the quaternary complex by the addition of SECIS (**Figure 2c**) indicates a preferential order for binding, *i.e*. GTP-activated SelB must recognize and preferentially interact with tRNA^{Sec} before recognizing the SECIS element.

Also, the tRNA^{Sec}-dependence to SECIS binding was analyzed by qualitative electrophoretic mobility shift assays (**Supplementary Figure 5**) similar to previously performed by Baron and collaborators [37]. GTP-activated SelB was previously incubated with fluorescein-labeled tRNA^{Sec} at different stoichiometric ratios. The presence of larger species representing SelB.GTP.tRNA^{Sec} is detected in comparison with unbound tRNA^{Sec} and SelB.GTP controls. Interestingly, this effect was also observed in the quaternary complex assembling SelB.GTP.tRNA^{Sec}.SECIS. However, SelB.GTP.SECIS interaction using fluorescein-labeled SECIS is not detectable, indicating the absence of the ternary complex. Therefore, as previously observed using fluorescence anisotropy, the quaternary complex formation is obtained by a sequence of specific bindings events.

SelB thermal unfolding, measured by Differential Scanning Calorimetry (DSC) (**Supplementary Figure 6**) has shown an enthalpy change (ΔH_{cal}) of (210 ± 10) kcal/mol and a melting temperature T_m of (47.4 ± 0.2) ºC. GTP binding to SelB does not change ΔH_{cal} of the binary systems (220 ± 20) and slightly increases the T_m in (0.8 ± 0.2) ºC. To evaluate the thermal stability of the ternary and quaternary complexes, the T_m of SelB.GTP was used as a reference upon complex formation. This analysis allowed the identification of two different groups of thermal stabilization ($\Delta T_m > 0$) and thermal destabilization ($\Delta T_m < 0$). The first group of tRNA^{Sec}, SECIS element, and its complexes, also tRNA$^{Sec}_{T\psi C}$ and tRNA$^{Sec}_{Anticodon}$ contains the samples whose ternary or quaternary complexes are more stable than SelB.GTP (**Table 5**). On the other hand, the second group was

formed by complexes, both $tRNA^{Sec}$ -variable arm variants, $tRNA^{Sec}_{D\text{-}loop,}$ and $tRNA^{Sec}_{acceptor}$, also the negative control $tRNA^{Ala}$, evidencing the formation of less thermally stable complexes.

Moreover, previous structural studies provided important snapshots from bacterial SelB [30,31], however, have not investigated the dynamic interactions of complex formation. To understand the structural modifications upon complex formation, *Fourier* transform infrared spectroscopy (FTIR) was performed, monitoring SelB secondary structures by amide-I normal mode absorption [17,38].

The secondary structure content obtained by FTIR spectra (**Supplementary Figure 7**) deconvolution is represented in **Table 6**. GTP-activated SelB contains 44% β-sheets, 16% α-helix, 16% turns, and approximately 23% random structures, consistent with its crystal structure [30]. In contrast, the ternary complex SelB.GTP.$tRNA^{Sec}$ showed an increase in α-helix structures (38%) and a proportional loss of β-sheet structure. Interestingly, the quaternary complex SelB.GTP.$tRNA^{Sec}$.SECIS does not show a considerable variation in secondary structure components, which indicates a secondary structural movement to accommodate the $tRNA^{Sec}$, consequently resulting in a suitable conformation for SECIS interaction. Therefore, imposing a sequential interaction, *i.e.*, SelB.GTP first interacts with $tRNA^{Sec}$ and SelB.GTP.$tRNA^{Sec}$ becomes competent to interact with the SECIS sequence.

The absence of structural information from SelB bound to its specific RNAs remains unsolved. To obtain structural information of the complexes, the surface interaction mapping was determined using hydrogen/deuterium exchange (HDx) followed by the molecular envelope determination by small-angle X-ray scattering (SAXS).

As shown in **Figure 3a**, 38 peptides were identified corresponding to 52% of coverage of the SelB primary structure. Mapping these peptides to the SelB tridimensional homology model, it was possible to identify the C-terminal domain*, i.e*. WHD3 and WHD4, as the most solvent accessible, in comparison with other regions (**Figure 3b**). SelB.GTP.$tRNA^{Sec}$ complex shows a drastic decrease of deuterium incorporation in the P37-L48, T184-L300 (WHD2), T429-L480 (WHD3), and P481-K641 (WHD4) regions (**Figure 3c**). Lately, the quaternary complex confirmed the SECIS recognition domain (WHD4) occlusion in the presence of the SECIS element (**Figure 3b**).

Deuterium incorporation mapping contributed to properly adjust the structural models into the SAXS molecular envelopes. Maximum molecular dimension, and gyration radii are represented in **Table 7**, highlighting the complexes formation. Molecular models were generated by the pairs-distribution function (**Supplementary Figure 8**) and superposed with the *E. coli* SelB homolog

model interacting with $tRNA^{Sec}$ and SECIS element as determined by HDx (**Figure 4**). These complexes present high flexibility in solution, as observed using the *Kratky* plot (**Supplementary Figure 9**).

Understanding the interactions with Sec pathway partners

According to the present models, $tRNA^{Sec}$ interacts with SelA after the Ser to Sec conversion and is transferred to SelB. In order to understand this interaction, SelB.GTP was titrated to fluorescein-labeled $tRNA^{Sec}$ in SelA.$tRNA^{Sec}$ binary complex. *E. coli* selenocysteine synthase (*Ec*SelA) and its binary complex were prepared as previously established [16,17,39].
The SelA.$tRNA^{Sec}$..SelB.GTP complex interacts with a K_D of (72 ± 14) nM (**Figure 5a**). In addition, FA experiments were performed to characterize the transfer of $tRNA^{Sec}$ to the ribosome summarized in **Table 4**. Initially, *E. coli* ribosome was titrated to SelB.GTP.$tRNA^{Sec}$ complex containing fluorescein-labeled $tRNA^{Sec}$, resulting in an observed K_D of (84 ± 6) nM (**Figure 5b**). Likewise, previously fluorescein-labeled SECIS complexed with SelB.GTP was titrated with increasing concentrations of ribosome until the expected binding saturation was reached. The binding profile revealed a K_D of (110 ± 9) nM, higher than that for SelB.GTP.$tRNA^{Sec}$ (**Figure 5c**). Lastly, the quaternary complex SelB.GTP.$tRNA^{Sec}$.SECIS containing fluorescein-labeled $tRNA^{Sec}$ was tested with increasing concentrations of the ribosome. A drastically lower K_D of (21 ± 2) nM was determined, indicating a four-fold higher affinity (**Figure 5d**). The same experimental conditions were evaluated by HPLC to ensure the absence of GTP cleavage during the ribosome binding assays (**Supplementary Figure 10**).

DISCUSSION

As previously described for the Sec biosynthesis pathway, molecular interactions are essential as key checkpoints that allow the proper delivery of $tRNA^{Sec}$ [11], and several of these interactions were already described for *Bacteria* [16,17,26,31,34,40], however, some interactions were unclear until this moment.

Sec, like any other amino acid, requires highly specific elongation factors for its proper delivery to the ribosome during translation. Bacterial SelB is responsible for decoding the UGA-Sec codon downstream to the mRNA SECIS also specifically recognizes the $tRNA^{Sec}$. *E. coli* SelB is activated by GTP binding, which allows the mature Sec-$tRNA^{Sec}$ interaction in complex with SelA with a high affinity (**Table 4**). SelB.GTP $tRNA^{Sec}$ recognition is facilitated by the presence of SelA, given

the low value obtained for the constant and cooperativity in interaction. These low-concentration values for interaction are biologically reasonable given that $tRNA^{Sec}$ is not abundant in the cell environment and the transfer must be extremely efficient due to the high toxicity of selenium compounds [3,14,41].

Fluorescence anisotropy and analytical ultracentrifugation revealed the specific recognition of the $tRNA^{Sec}$ variable arm (**Figure 1** and **Supplementary Figure 3**). We observed lower K_D values for acceptor-TΨC helix and the variable arm variants in comparison with wild-type $tRNA^{Sec}$. These $tRNA^{Sec}$ recognition elements are complementary to SelA recognition between the acceptor stem and D-loop [15] and are the same as those that interact with SerRS, responsible for the tRNA aminoacylation [34].

Mapping SelB interactions regions, HDx mapped the occlusion of WHDs II and III (**Figure 3**), in agreement with previously cryo-EM complex reconstruction observed in complex with the ribosome [31]. This indicates that, in solution, SelB.$tRNA^{Sec}$ complex remains attached in a conserved conformation even after SECIS interaction. Consistent with this sequence of events, additional evidence suggested that SelB presents a *folding-upon-binding* mechanism after $tRNA^{Sec}$ interaction [31,42,43].

Analysis of the complexes thermal stability by DSC shows two different groups (**Supplementary Figure 6** and **Table 5**). The formation of the binary samples SelB.$tRNA^{Sec}$ and SelB.GTP along with the ternary complexes formed by SelB.GTP with $tRNA^{Sec}$, the TψC, and anticodon arms variants, SECIS, and SECIS.$tRNA^{Sec}$ yielded more thermally stable complexes than SelB. On the other hand, the protein-nucleotide complexes composed of the variable arm mutants, D-loop, acceptor stems, and $tRNA^{Ala}$, used as a negative control, showed a negative displacement of the T_m, indicating less thermally stable complexes compared to SelB. The latter is likely due to incorrect packing, as observed by AUC (**Supplementary Figures 3 and 4**).

SelB-RNAs complexation can be partially related to secondary structure variation observed during the ternary and quaternary complex formation (**Supplementary Figure 7**). During RNAs binding, an increase in α-helix and a decrease in unordered structures of SelB were detected. These structure variations must occur on WHD2/3 and WHD4, which are the regions that specifically recognize the $tRNA^{Sec}$ and SECIS, respectively. The sequence of WHD2 (T184-L300) and the initial portion of WHD3 (T429-L450) are responsible for interacting with the acceptor and TψC stems (**Figure 3** and **Figure 4**). Moreover, the WHD3 final sequence (P451-L480), responsible for the variable arm recognition, is occluded during SelB.GTP.$tRNA^{Sec}$ complex formation.

The SECIS element interacts with the WHD4 domain, resulting in a decrease in deuterium incorporation on this portion (**Figure 3c**). These interaction models are also consistent with low-resolution models obtained by SAXS analysis, where the D_{max} and interaction points (variable arm in $tRNA^{Sec}$ and WHD3 and WHD4 in SelB) validate the proposed macromolecular complex *in solution* and show the specificity of the tRNA as a recognition element in this specific biochemical pathway. These results revealed that SelB undergoes conformational changes due to the interaction with RNAs, as shown by SAXS from EFSec [32] and the high-resolution reconstruction models obtained by cryo-electron microscopy [31].

Another key discovery from this report is the sequence of events during Sec-$tRNA^{Sec}$ biosynthesis and incorporation. The interaction of the complex with SelB.GTP.$tRNA^{Sec}$.SECIS has a high affinity (**Figure 5**) when compared with the other combinations, showing that the previously assembled SelB.GTP.$tRNA^{Sec}$ complex has a favorable interaction in comparison with the formation of the complex in the presence of SECIS. Therefore, activated SelB recognizes $tRNA^{Sec}$ resulting in SelB.GTP.$tRNA^{Sec}$ complex that subsequently recognizes the SECIS element for $tRNA^{Sec}$ delivery to the ribosome (**Figures 5c-d**). This model is based on the affinity constant values and a qualitative electrophoretic mobility shift (**Supplementary Figure 5**), which shows the SelB.GTP.$tRNA^{Sec}$.SECIS quaternary complex formation in the presence of both RNAs elements. Taken together, our results support the pathway in which the mature $tRNA^{Sec}$ in complex with SelA is specifically recognized and then transferred to the activated SelB and subsequently, this ternary complex can recognize the SECIS element and properly deliver the Sec-$tRNA^{Sec}$ to the ribosome for its incorporation into the nascent protein (**Figure 6**).

MATERIALS AND METHODS

Specific elongation factor (SelB) purification and initial characterization

The vector containing the gene *selB* with hexahistidine-tag at the C-termini, referred to as pT7-6-*selB*H6 (4523 pb) [10,31], was kindly provided by Prof. Dr. Marina Rodnina (Department of Physical Biochemistry - Max Planck Institute for Biophysical Chemistry – Göttingen - Germany) and transformed into *E. coli* BL21 (λ-DE3). The cells were grown in agitation at 37 ºC, 150 rpm during 6 h in LB media containing ampicillin (25 µg/mL) until the optical density ($O.D._{.600nm}$) of 1.0 was obtained, for induction with 0.5 mM isopropyl β-*D*-1-thiogalactopyranoside (IPTG) for 3 h at 37 °C. The cells were harvested at 2,000 xg for 45 min at 4 ºC and the pellet was suspended in 200 mM H_3BO_3 pH 7.0 supplemented with 10 mM $MgCl_2$ followed by centrifugation at 13,000 rpm for 45 min at 4 ºC as previously established by Thanbichler and Böck [41].

The cell pellet was suspended in 200 mM H_3BO_3 pH 7.0 supplemented with 10 mM $MgCl_2$, 1 M NaCl, 200 µg/µL phenylmethanesulfonylfluoride (PMSF) and 1 mM 2-mercaptoethanol in the proportion of 1 mL per gram of dry cells. The cell lysis was performed by the addition of lysozyme (50 µg/mL, Millipore Sigma) and incubation for 30 min on ice and, subsequently, disrupted by sonication pulses followed by centrifugation at 2,000 xg for 30 min at 4 ºC. The clarified extract was submitted to affinity chromatography using pre-equilibrated Cobalt-affinity chromatography (Qiagen). The sample was subsequently washed and eluted in the same buffer with imidazole concentrations of 10 mM and 100 mM, respectively.

Endogenous co-purified RNAs were determined by Qubit fluorometer (Invitrogen) using the Quanti-tRNA assay [29,39] and were subsequently removed by 12 h treatment with 10 µg/mL RNAse A (Life Technologies) per microgram of purified SelB at 4 ºC. SelB was dialyzed in 100 mM potassium phosphate pH 7.0, 5 mM magnesium sulfate, 0.5 mM ethylenediaminetetraacetic acid (EDTA), 150 mM sodium chloride and submitted to size-exclusion chromatography (SEC) using Superdex 75 (10/30) column. All the steps were monitored by 15% SDS-PAGE that was used for characterization by western-blot and mass spectrometry sequencing, following a protocol previously established [44].

Finally, High-Performance Liquid Chromatography (HPLC) was performed as a sensitive technique to detect the presence of endogenous nucleotides and its consumption as time or complexes dependence, such as in complex with the specific RNAs (unacylated-$tRNA^{Sec}$ and SECIS) and ribosome [45]. For this, 20 µM of SelB was conducted also with precooled 1.5 M $HClO_4$ and incubated for 10 min at 4 ºC. Denatured proteins were precipitated by centrifugation at 16,000 xg for 10 min at 4 ºC. Then, 100 µL KOH [3 M], 80 µL CH_3COOH [5 M], and 100 µL K_2HPO_4 [1M] were added in 600 µL of supernatant collected and stored at -20 °C [46]. The nucleotide's controls were prepared at 100 µM and the RNAs and ribosome concentration were kept constant around 20 µM. The samples were analyzed by ion-exchange column Protein Pack DEAE 5 PW, 7.5 mm x 7.5 cm (Waters) pre-equilibrated with 100 mM potassium phosphate pH 7.0, 100 mM NaCl and the nucleotides absorbance was monitored at 253 nm. GTP hydrolysis was monitored for 60 min at 25 °C and the chromatograms were obtained by a linear gradient of 100-900 mM NaCl and analyzed using Origin 8.5 (OriginLab) software.

Amplifying and obtaining the specific RNAs

To elucidate which regions of $tRNA^{Sec}$ are determinant for the interaction with SelB protein, $tRNA^{Sec}$ variants were synthesized and subjected to fluorescence anisotropy (FA) assays [16,17,34]. The *E. coli* $tRNA^{Sec}$ and its variants were amplified by PCR, *in vitro* transcribed and, subsequently, labeled with fluorescein maleimide as prescribed [16,34]. The oligonucleotides of $tRNA^{Sec}$ variants were designed with specific replacements corresponding to similar regions presented in amino acid serine tRNA ($tRNA^{Ser}$) from *E. coli* as described by Silva and collaborators [17]. The regions of $tRNA^{Sec}$ that acquired a replacement for the similar nucleotides presented in $tRNA^{Ser}$ are the acceptor arm, anticodon arm, D-loop arm, variable arm, and TψC arm.

Also, the $tRNA^{Ala}$ was amplified as a negative control using the following oligonucleotides:

ala-forward:

5'TAATACGACTCACTATAGGGGATGTAGCTCAGATGGTAGAGCGCCCGCTTAGCATGCG3'

ala-reverse:

5'TTGTGGAGAAGTTGGGTATCGATCCCAATACCTCCCGCATGCTAAGCGGGCGCTC3'

The same procedure was also applied to obtain one of the type-1 SECIS elements from *E. coli* formate dehydrogenase-H (FDH-H) selenoenzyme [47].

secis-forward:

5'GCTAATACGACTCACTATAGGGAGCAGCAGGAUGAGGGC3'

secis-reverse:

5'CTTGGCGGTGCAGACCTGCAACCGCCCTCATCCTGCTGC3'

SECIS-transcript:

5'CGAUUAUGCUGAGUGAUAUCCCUCGUCGUCCUCUCCCG3'

The transcript presents 39 nucleotides and the secondary structure generated by RNAfold web server [48] and represented in Figure 2d.

The folding of *in vitro* translated $tRNA^{[Ser]Sec}$ was monitored by circular dichroism in J-815 spectropolarimeter (JASCO Corporation, Japan) showing the characteristic "S" profile of correctly folded nucleic acids and a maximum observed peak at 268 nm, as previously established [16,17,34]. The thermal folding assays were observed using 20 μM of RNA in $RNase_{free}$ water with the addition of 20 mM $MgCl_2$.The wavelength monitored 210-320 nm with an average of 8 scans with a resolution of 1 nm acquired at 50 nm/min with a temperature range from 10 °C to 90 °C at a rate of 1 °C/min. Data were processed using the Origin 8.5 program and the Boltzmann function was used to evaluate the thermal folding [34,49,50].

Selenocysteine synthetase expression and purification

Selenocysteine synthase (SelA) has been extensively studied and its expression and purification protocol were previously established by Manzine *et al.* [16,39]. The *selA* gene was inserted in pET29a (+) vector and transformed into *E. coli* WL81640 (λ-DE3). Briefly, cells were grown for 3 h until $O.D._{600nm}$ 1.0 and induced with 0.1 mM IPTG. After cell lysis by sonication, the protein extract was submitted into salting-out 25% ammonium sulfate precipitation followed by size exclusion chromatography in buffer 20 mM potassium phosphate pH 7.5, 100 mM sodium chloride, 5% glycerol, 2 mM β-mercaptoethanol, and 10 μM pyridoxal 5'-phosphate (PLP). The protein purity was evaluated from SDS-PAGE analysis.

Macromolecular binding assays using fluorescence anisotropy spectroscopy (FA)

The RNAs molecules were covalently labeled with fluorescein-5-maleimide using the commercial 5' EndTagTM Nucleic Acid Labeling System kit (Vector Laboratories, Burlingame, CA, USA) [16,17,34]. Fluorescence anisotropy measurements were performed in biological triplicates using an ISS-PC spectrofluorometer (ISS, Champaign, IL) in "L" geometry with single-channel monitoring the emission at 520 nm and excitation at 492 nm.

Unacylated-$tRNA^{Sec}$ and its variant interactions were conducted using 49 nM unlabeled tRNA and 1 nM fluorescein labeled-tRNA incubated in a quartz cuvette of 1 cm path at 25 °C in presence of 100 mM GTP. Subsequently, increasing concentrations of SelB were titrated and anisotropy measurements have collected an average of 5 interactions. All the titrations were homogenized and equilibrated for 10 min to reach thermal equilibrium. The results were processed by Origin 8.5 software and, after normalization, adjusted using the *Hill* equation to obtain the apparent dissociation constant (K_D) and cooperativity index (*n*) [51] according to the following equation:

$$\boldsymbol{r = r_0 + (r_f - r_0)\, x \frac{([SelB])^n}{(K_D)^n + ([SelB])^n}}$$

where, *r* is the anisotropy value (r_0 and r_f correspond to initial and final anisotropy values, respectively), and [SelB] is the SelB concentration added in the cuvette. The same experimental procedures were applied to SelB binding assays against SECIS fluorescein-labeled [1 nM] in presence of SECIS element [49 nM] and GTP [100 mM].

The quaternary complex formation (SelB.GTP.$tRNA^{Sec}$.SECIS) was also determined using the same method. SelB.$tRNA^{Sec}$ pre-assembled in equimolar stoichiometry was titrated in SECIS

fluorescein-labeled [1 nM] in presence of SECIS element [49 nM] and 100 mM GTP. The sequential order was evaluated using the same procedure, where SelB.SECIS pre-assembled in equimolar stoichiometry were sequentially added in 49 nM unlabeled $tRNA^{Sec}$ and 1 nM fluorescein-labeled $tRNA^{Sec}$ at the same experimental conditions.

Sequentially, analysis of SelB interaction with previously assembled binary complex SelA.$tRNA^{Sec}$ was performed as previously described [16,17]. 50 nM SelA was previously incubated for 10 min at 25 °C in equimolar stoichiometry with $tRNA^{Sec}$ (49 nM unlabeled and 1 nM fluorescein-labeled $tRNA^{Sec}$). The same experimental procedures were followed as described for the tRNAs binding assays.

The SelB.GTP.$tRNA^{Sec}$.SECIS.ribosome interaction was demonstrated by increasing ribosome concentration following the workflow previously described. *E. coli* ribosome complex (NEB, P0763S – 13.3 μM) was prepared in 100 mM potassium phosphate pH 7.0, 5 mM magnesium sulfate, 0.5 mM EDTA and 150 mM sodium chloride. All average values and standard deviations were calculated using experimental triplicates using 100 mM GTP and the final analysis was represented in normalized (0-1) anisotropy values.

Analysis of the $tRNA^{Sec}$ variant's complexes formation by analytical ultracentrifugation

The analytical ultracentrifugation (AUC) experiments were performed in Beckman Coulter Proteome Lab XL-I (Beckman Coulter) with a Proteome Lab XL-I (220-240 VAC, 50 Hz) rotor in the Spectroscopy and Calorimetry Laboratory (LEC) of the Brazilian Center for Research in Energy and Materials (CNPEM). AUC analysis followed the protocol established by Scortecci and collaborators [40]. Five unique $tRNA^{Sec}$ variants with the most relevant contributions to the SelB interaction were selected: acceptor, D-loop, TψC, variable arms, and unacylated-$tRNA^{Ala}$ as a negative control. SelB and the SelB-tRNAs complexes were tested at a concentration of 9.8 μM and 3.5 μM, respectively. The sedimentation velocity experiments were performed at 40,000 rpm at 25 ºC and monitored at 280 nm for 26 h. The theoretical values for the constants related to the density and viscosity from the experimental buffer were calculated by Sednterp program. For interpretation of radial absorption, the resulting curves were fitted by Sedfit program using the *Lamm* equation with a continuous distribution *c(S)* model [52,53].

The sedimentation equilibrium analysis was carried out at 25 °C in steps of 8,000 rpm; 12,000 rpm; 15,000 rpm and 18,000 rpm for 12 h each velocity to ensure the sedimentation equilibrium

before the 280 nm absorption measurement. The $tRNA^{Sec}$ constructs were constant at 3.5 μM and different concentrations of SelB were added to give the final molar ratio of 0.5:1, 1:1, and 2:1 (SelB:tRNA), respectively. Sedphat software was employed using model (A + B = AB).

Qualitative electrophoretic mobility shift assays under native conditions.

SelB complexes formation was also monitored by a qualitative electrophoretic mobility shift assay under native conditions. The 2% agarose RNA_{free} gel was stained with 10% SyBr Safe (Thermofisher) and the RNAs fluorescein-labeled samples at 1 μM and the SelB.GTP was titrated in stoichiometric ratios (1:0.5; 1:1 and 1:2). The gel was submitted to 80 V, 400 mA for 120 minutes at 4 °C, and the results were observed using the Gel DocTM XR+ Gel documentation system (BioRad) at 470 nm.

Thermal stability analysis by differential scanning calorimetry (DSC)

DSC was also employed to characterize the stability of SelB and its complexes with GTP and the RNAs through the determination of the unfolding transition temperature, T_m, and the associated unfolding enthalpies [54]. Experiments were carried out on a VP-DSC MicroCal MicroCalorimeter (Microcal, Northampton, MA, USA) with a heating rate of 63.4 °C/h in a temperature range from 10 °C to 65 °C and at constant pressure (1 atm). DSC thermograms of SelB and its complexes were recorded only during the first heating scan since protein aggregates after unfolding. 7 μM SelB was used with an excess of GTP (100 mM), $tRNA^{Sec,}$ and its variants (14 μM), and SECIS (12 μM). After instrumental buffer baseline subtraction and baseline correction, the resulting thermograms were normalized to the protein molar concentration and deconvoluted using Microcal Origin DSC software.

Secondary structure variation monitored by *Fourier* transform infrared spectroscopy

In solution samples infra-red spectra were collected using Spectrum Two-IR spectrometer (Perkin Elmer) with DTGS detector by 10 accumulations at 25 °C for 300 seconds. This data has 2 cm^{-1} of resolution and a wavenumber range of 4000-400 cm^{-1}. The buffer spectrum was subtracted from the sample's datasets. The analyzed samples: SelB.GTP; SelB.GTP.$tRNA^{Sec}$ and SelB.GTP.$tRNA^{Sec}$.SECIS were assembled at 10 μM SelB; 12 μM to RNAs and 100 μM GTP,

respectively. The second derivative was used to identify the peak positions of the amide I band on the protein vibrational spectra average. The secondary structure percentage was obtained by *Gaussian* fitting performed in 1700-1600 cm^{-1} range. The difference in infrared spectra was used to monitor the difference between SelB bound and unbound states with RNAs during complexes formation, subtracting the complex spectra from isolated SelB.GTP [17,38].

E. coli SelB homology model

The structural model of *E. coli* SelB was obtained using I-TASSER web server [55], where was applied multiple threading and homology modeling rounds using the *A. aeolicus* crystallographic structure as a template (PDB.ID 4ZU9) [30]. The SelB interacting with the $tRNA^{Sec}$ model was obtained by rigid body superposition using the crystallographic $tRNA^{Sec}$ structure (PDB. ID 3A3A) and the SelB interacting with both RNAs (SECIS element addition) was obtained using structural alignment with the C-terminal domain in complex with SECIS element (PDB.ID 2PJP).

Hydrogen-deuterium exchange analyzed by mass spectrometry (HDx)

The hydrogen-deuterium exchange coupled with mass-spectrometry analysis was applied to map the surface of SelB when interacting with GTP; $tRNA^{Sec}$ and SECIS element. The samples were prepared as followed by the protocol previously established [17]. The samples were labeled by the dilution in 75% D_2O solution using 2 different incubation times (5 and 30 min). 2.6 µM of SelB was diluted in 20 mM potassium phosphate pH 2.0 formic acid added and sequentially incubated with 0.6 µM of pepsin (Sigma-Aldrich) for 10 min at 25 °C. Then, the sample was applied to an ESI-microTOF QII (Q-TOF) mass spectrometer (Bruker Daltonik) at a flow rate of 240 µL/h. The SelB.GTP; SelB.GTP.$tRNA^{Sec}$ and SelB.GTP.$tRNA^{Sec}$.SECIS complexes were prepared using 100 mM GTP and 10 µM of both RNAs ($tRNA^{Sec}$ and SECIS element). The mass spectra were acquired, treated, and analyzed using the algorithms HyStar version 3.2, Compass for otofControl version 1.7, and DataAnalysis version 4.3 (Bruker Daltonik). The *m/z* values corresponding to each peptide sequence detected were compared to each other, considering the presence and absence of HDx, permitting to assign the mass displacement peaks according to PeptideCutter server [56]. The results were plotted on the molecular model previously obtained by molecular modeling using Pymol 1.3 software (Schrodinger, LLC).

In solution model using small-angle X-ray scattering (SAXS)

Small-angle X-ray scattering (SAXS) analysis data were collected in SAXS1 beamline at National Synchrotron Laboratory (LNLS/CNPEM - Campinas, Brazil), with λ = 1.488 Å and a detector/sample distance of 1.033 mm, with a bi-dimensional position-sensitive Pilatus detector. The SAXS analyses of SelB were performed in three different conditions: SelB.GTP, SelB.GTP.tRNA^{Sec} and SelB.GTP.tRNA^{Sec}.SECIS at final concentrations of 2.2 mg/mL and 1.0 mg/mL of SelB and equimolar concentration of RNAs. All experiments were conducted at 25 ºC. The samples were exposed in frames of 30 seconds and the parasitic scattering was subtracted from sample scatterings and the data treatment was performed through the ATSAS program package [57,58]. The intensity values obtained directly from the experimental diffraction pattern were subtracted from the value of the *Porod* constant. The gyration radii (Rg) and the distance distribution function p(r) were obtained by GNOM [57]. From the scattering curves, low-resolution envelope *ab initio* models were generated through DAMMIF and fitted with the homology model using SUPCOMB [57]. The SAXS envelopes figures from SelB and complexes were generated in the PyMOL 1.3 (Schrodinger, LLC).

ACKNOWLEDGMENTS

We would like to thank Professor Marina Rodnina (Max Planck Institute) for kindly providing the plasmid containing the *selbH6-pT7* vector that made possible the realization of this study. This work was supported by the research grants from FAPESP (1998/14138-2; 2013/17791-0; VHBS - 2012/23730-1; LGMB – 2014/00206-0; JFS – 2012/15777-8 and 2014/16005-4); CNPq (550514/2011-2; AFF – 134013/2015-8; VHBS - 232251/2014-2 and 140636/2013-7) and CAPES. V.H.B.S. is the recipient of a Banting Postdoctoral Fellowship. We would like to thank the “Sergio Mascarenhas” Biophysics Group (IFSC/USP), LEC, and LNLS from CNPEM (Brazil) for providing experimental support. We also acknowledge Dr. Fernanda A. H. Baptista and Dr. Ana Carolina M. Figueira from National Laboratory of Biosciences (LNBio/CNPEM) for the AUC measures; Prof. Júlio César Borges from Sao Carlos Chemistry Institute (IQSC/USP) for AUC data analysis, Prof. Mário de Oliveira Neto from Sao Paulo State University (UNESP) and the National Laboratory of Synchrotron Radiation (LNLS/CNPEM) for SAXS measurements and analysis, and Dr. Ana Laura Lima (Structural Biology Lab - LBEst) for art design. A special acknowledgment to Dr. Livia R. Manzine for helping in data treatment and for the tRNA$^{[Ser]Sec}$ constructs used in this work. We would like to acknowledge Derminda Isabel de Moraes, Dr. Humberto D’Muniz Pereira, Dr. Andressa Patricia Alves Pinto, and Dr. Susana Andrea Sculaccio Beozzo from the Sao Carlos Institute of Physics, University of Sao Paulo as well as all members from the structural biology laboratory for their contributions.

AUTHOR CONTRIBUTIONS

V.H.B.S. - Conceptualization; Data curation; Formal analysis; Investigation; Methodology; Project administration; Roles/Writing - original draft. A.F.F. - Conceptualization; Data curation; Formal analysis; Investigation; Methodology; Roles/Writing - original draft. L.G.M.B. - Data curation; Formal analysis; Methodology; Roles/Writing - original draft. J.F.S. - Data curation; Formal analysis; Methodology; Roles/Writing - original draft. E.C.J. - Data curation; Formal analysis. M.L.C - Data curation; Formal analysis; Methodology. B.M.S. - Data curation; Formal analysis; Methodology. M.S.P - Methodology; Resources. M.O.N. - Data curation; Formal analysis; Methodology; Validation; Visualization. O.H.T. – Conceptualization; Funding acquisition; Project administration; Resources; Supervision; Validation; Visualization; Roles/Writing - original draft.

REFERENCES

[1] I.M. Krab, A. Parmeggiani, Mechanisms of EF-Tu, a pioneer GTPase, Progress in Nucleic Acid Research and Molecular Biology. 71 (2002) 513–551. https://doi.org/10.1016/s0079-6603(02)71050-7.

[2] G.R. Andersen, P. Nissen, J. Nyborg, Elongation factors in protein biosynthesis, Trends in Biochemical Sciences. 28 (2003) 434–441. https://doi.org/10.1016/S0968-0004(03)00162-2.

[3] C. Böck, A., Forchhammer, K., Heider, J., & Baron, Selenoprotein synthesis: an expansion of the genetic code, Trends in Biochemical Sciences. (1991) 463–467. https://doi.org/10.1016/0968-0004(91)90180-4.

[4] M. Leibundgut, C. Frick, M. Thanbichler, A. Böck, N. Ban, Selenocysteine tRNA-specific elongation factor SelB is a structural chimaera of elongation and initiation factors, EMBO Journal. 24 (2005) 11–22. https://doi.org/10.1038/sj.emboj.7600505.

[5] G.C. Atkinson, V. Hauryliuk, T. Tenson, An ancient family of SelB elongation factor-like proteins with a broad but disjunct distribution across archaea, BMC Evolutionary Biology. 11 (2011) 1–10. https://doi.org/10.1186/1471-2148-11-22.

[6] J. Lu, A. Holmgren, Selenoproteins, Journal of Biological Chemistry. 284 (2009) 723–727. https://doi.org/10.1074/jbc.R800045200.

[7] L.V. Papp, J. Lu, A. Holmgren, K.K. Khanna, From selenium to selenoproteins: Synthesis, identity, and their role in human health, Antioxidants and Redox Signaling. 9 (2007) 775–806. https://doi.org/10.1089/ars.2007.1528.

[8] S. Yoshizawa, A. Böck, The many levels of control on bacterial selenoprotein synthesis, Biochimica et Biophysica Acta - General Subjects. 1790 (2009) 1404–1414. https://doi.org/10.1016/j.bbagen.2009.03.010.

[9] J.E. Squires, M.J. Berry, Eukaryotic selenoprotein synthesis: Mechanistic insight incorporating new factors and new functions for old factors, IUBMB Life. 60 (2008) 232–235. https://doi.org/10.1002/iub.38.

[10] T. Mukai, M. Englert, H.J. Tripp, C. Miller, N.N. Ivanova, E.M. Rubin, N.C. Kyrpides, D. Söll, Facile Recoding of Selenocysteine in Nature, Angewandte Chemie - International Edition. 55 (2016) 5337–5341. https://doi.org/10.1002/anie.201511657.

[11] V.H.B. Serrão, I.R. Silva, M.T.A. da Silva, J.F. Scortecci, A. de Freitas Fernandes, O.H. Thiemann, The unique $tRNA^{Sec}$ and its role in selenocysteine biosynthesis, Amino Acids. 50 (2018). https://doi.org/10.1007/s00726-018-2595-6.

[12] J.F. (2020). Serrão, V. H. B., & Scortecci, Why Selenocysteine Is Unique?, Frontiers in Molecular Biosciences. 7 (2020) 1–3. https://doi.org/10.3389/fmolb.2020.00002.

[13] M.A.R. Gomez, M. Ibba, Aminoacyl-tRNA synthetases, Current Opinion in Structural Biology. 2 (1992) 138–142. https://doi.org/10.1016/0959-440X(92)90189-E.

[14] K. Forchhammer, A. Bock, Selenocysteine synthase from Escherichia coli: Analysis of the reaction sequence, Journal of Biological Chemistry. 266 (1991) 6324–6328. https://doi.org/10.1016/s0021-9258(18)38121-3.

[15] D. Sela, Decameric SelA • tRNA, 340 (2013) 75–79.

[16] L.R. Manzine, V.H.B. Serrão, L.M.T.D.R.E. Lima, M.M. De Souza, J. Bettini, R.V. Portugal, M. Van Heel, O.H. Thiemann, Assembly stoichiometry of bacterial selenocysteine synthase and SelC (tRNAsec), FEBS Letters. 587 (2013) 906–911. https://doi.org/10.1016/j.febslet.2013.02.014.

[17] I.R. Silva, V.H.B. Serrão, L.R. Manzine, L.M. Faim, M.T.A. Da Silva, R. Makki, D.M. Saidemberg, M.L. Cornélio, M.S. Palma, O.H. Thiemann, Formation of a ternary complex for selenocysteine biosynthesis in bacteria, Journal of Biological Chemistry. 290 (2015) 29178–29188. https://doi.org/10.1074/jbc.M114.613406.

[18] R. Walczak, E. Westhof, P. Carbon, A. Krol, A novel RNA structural motif in the selenocysteine insertion element of eukaryotic selenoprotein mRNAs, Rna. 2 (1996) 367–379.

[19] A. Krol, Evolutionarily different RNA motifs and RNA-protein complexes to achieve selenoprotein synthesis, Biochimie. 84 (2002) 765–774. https://doi.org/10.1016/S0300-9084(02)01405-0.

[20] R. Hilgenfeld, A. Böck, R. Wilting, Structural model for the selenocysteine-specific elongation factor SelB, Biochimie. 78 (1996) 971–978. https://doi.org/10.1016/S0300-9084(97)86719-3.

[21] M. Kromayer, R. Wilting, P. Tormay, A. Böck, Domain structure of the prokaryotic selenocysteine-specific elongation factor SelB, Journal of Molecular Biology. 262 (1996) 413–420. https://doi.org/10.1006/jmbi.1996.0525.

[22] S. Yoshizawa, L. Rasubala, T. Ose, D. Kohda, D. Fourmy, K. Maenaka, Structural basis for mRNA recognition by elongation factor SelB, Nature Structural and Molecular Biology. 12 (2005) 198–203. https://doi.org/10.1038/nsmb890.

[23] S.J. Klug, A. Hüttenhofer, M. Kromayer, M. Famulok, In vitro and in vivo characterization of novel mRNA motifs that bind special elongation factor SelB, Proceedings of the National Academy of Sciences of the United States of America. 94 (1997) 6676–6681. https://doi.org/10.1073/pnas.94.13.6676.

[24] V.E. Deley Cox, M.F. Cole, E.A. Gaucher, Incorporation of Modified Amino Acids by Engineered Elongation Factors with Expanded Substrate Capabilities, ACS Synthetic Biology. 8 (2019) 287–296. https://doi.org/10.1021/acssynbio.8b00305.

[25] O. Vargas-Rodriguez, M. Englert, A. Merkuryev, T. Mukai, D. Söll, Recoding of the selenocysteine UGA codon by cysteine in the presence of a non-canonical tRNACys and elongation factor SelB, RNA Biology. 15 (2018) 471–479. https://doi.org/10.1080/15476286.2018.1474074.

[26] A. Paleskava, A.L. Konevega, M. V. Rodnina, Thermodynamic and kinetic framework of selenocysteyl-tRNASec recognition by elongation factor SelB, Journal of Biological Chemistry. 285 (2010) 3014–3020. https://doi.org/10.1074/jbc.M109.081380.

[27] P.J. Keeling, N.M. Fast, G.I. McFadden, Evolutionary relationship between translation initiation factor eIF-2γ and selenocysteine-specific elongation factor SELB: Change of function in translation factors, Journal of Molecular Evolution. 47 (1998) 649–655. https://doi.org/10.1007/PL00006422.

[28] A. Hüttenhofer, A. Böck, Selenocysteine inserting RNA elements modulate GTP hydrolysis of elongation factor SelB, Biochemistry. 37 (1998) 885–890. https://doi.org/10.1021/bi972298k.

[29] C. Baron, A. Bock, The length of the aminoacyl-acceptor stem of the selenocysteine-specific tRNA(Sec) of Escherichia coli is the determinant for binding to elongation factors SELB or Tu, Journal of Biological Chemistry. 266 (1991) 20375–20379. https://doi.org/10.1016/s0021-9258(18)54933-4.

[30] Y. Itoh, S.I. Sekine, S. Yokoyama, Crystal structure of the full-length bacterial selenocysteine-specific elongation factor SelB, Nucleic Acids Research. 43 (2015) 9028–9038. https://doi.org/10.1093/nar/gkv833.

[31] N. Fischer, P. Neumann, L. V. Bock, C. Maracci, Z. Wang, A. Paleskava, A.L. Konevega, G.F. Schröder, H. Grubmüller, R. Ficner, M. V. Rodnina, H. Stark, The pathway to GTPase activation of elongation factor SelB on the ribosome, Nature. 540 (2016) 80–85. https://doi.org/10.1038/nature20560.

[32] M. Dobosz-Bartoszek, M.H. Pinkerton, Z. Otwinowski, S. Chakravarthy, D. Söll, P.R. Copeland, M. Simonovic, Crystal structures of the human elongation factor eEFSec suggest a non-canonical mechanism for selenocysteine incorporation, Nature Communications. 7 (2016). https://doi.org/10.1038/ncomms12941.

[33] M. V. Rodnina, N. Fischer, C. Maracci, H. Stark, Ribosome dynamics during decoding, Philosophical Transactions of the Royal Society B: Biological Sciences. 372 (2017). https://doi.org/10.1098/rstb.2016.0182.

[34] A. de Freitas Fernandes, V.H.B. Serrão, J.F. Scortecci, O.H. Thiemann, Seryl-tRNA synthetase specificity for tRNASec in Bacterial Sec biosynthesis, Biochimica et Biophysica Acta. Proteins and Proteomics. 1868 (2020) 140438. https://doi.org/10.1016/j.bbapap.2020.140438.

[35] V.A. Dell, A.E. Johnson, V.A. Dell, A.E. Johnson, V.A. Dell, D.L. Miller, Effects of Nucleotide- and Aurodox-Induced Changes in Elongation Factor Tu Conformation upon Its Interactions with Aminoacyl Transfer RNA. A Fluorescence Study, Biochemistry. 29 (1990) 1757–1763. https://doi.org/10.1021/bi00459a014.

[36] A. Paleskava, A.L. Konevega, M.V. Rodnina, Thermodynamic and Kinetic Framework of Selenocysteyl-tRNASec Recognition by Elongation Factor SelB, J. Biol. Chem. 285 (2010) 3014–3020. https://doi.org/10.1074/jbc.M109.081380.

[37] C. Baron, J. Heider, A. Böck, Interaction of translation factor SELB with the formate dehydrogenase H selenopolypeptide mRNA, Proceedings of the National Academy of Sciences of the United States of America. 90 (1993) 4181–4185. https://doi.org/10.1073/pnas.90.9.4181.

[38] H. Fabian, H.H. Mantsch, C.P. Schultz, Two-dimensional IR correlation spectroscopy: Sequential events in the unfolding process of the λ Cro-VSSC repressor protein, Proceedings of the National Academy of Sciences of the United States of America. 96 (1999) 13153–13158. https://doi.org/10.1073/pnas.96.23.13153.

[39] L.R. Manzine, A. Cassago, M.T.A. Da Silva, O.H. Thiemann, An efficient protocol for the production of tRNA-free recombinant Selenocysteine Synthase (SELA) from Escherichia coli and its biophysical characterization, Protein Expression and Purification. 88 (2013) 80–84. https://doi.org/10.1016/j.pep.2012.12.005.

[40] J.F. Scortecci, V.H.B. Serrão, A.F. Fernandes, L.G.M. Basso, R.F. Gutierrez, A.P.U. Araujo, M.O. Neto, O.H. Thiemann, Initial steps in selenocysteine biosynthesis: The interaction between selenocysteine lyase and selenophosphate synthetase, International Journal of Biological Macromolecules. 156 (2020) 18–26. https://doi.org/10.1016/j.ijbiomac.2020.03.241.

[41] M. Thanbichler, A. Böck, Purification and characterization of hexahistidine-tagged elongation factor SelB, Protein Expression and Purification. 31 (2003) 265–270. https://doi.org/10.1016/S1046-5928(03)00167-0.

[42] M. Simonović, A.K. Puppala, On elongation factor eEFSec, its role and mechanism during selenium incorporation into nascent selenoproteins, Biochimica et Biophysica Acta - General Subjects. 1862 (2018) 2463–2472. https://doi.org/10.1016/j.bbagen.2018.03.018.

[43] X. Fu, D. Söll, A. Sevostyanova, Challenges of site-specific selenocysteine incorporation into proteins by Escherichia coli, RNA Biology. 15 (2018) 461–470. https://doi.org/10.1080/15476286.2018.1440876.

[44] A. Shevchenko, H. Tomas, J. Havliš, J. V. Olsen, M. Mann, In-gel digestion for mass spectrometric characterization of proteins and proteomes, Nature Protocols. 1 (2007) 2856–2860. https://doi.org/10.1038/nprot.2006.468.

[45] V.H.B. Serrão, F. Alessandro, V.E.A. Caldas, R.L. Maral, H. D'Muniz Pereira, O.H. Thiemann, R.C. Garratt, Promiscuous interactions of human septins: The GTP binding domain of SEPT7 forms filaments within the crystal, FEBS Letters. 585 (2011) 3868–3873. https://doi.org/10.1016/j.febslet.2011.10.043.

[46] K.E. Robinson, J. Orans, A.R. Kovach, T.M. Link, R.G. Brennan, Mapping Hfq-RNA interaction surfaces using tryptophan fluorescence quenching, Nucleic Acids Research. 42 (2014) 2736–2749. https://doi.org/10.1093/nar/gkt1171.

[47] F. Zinoni, J. Heider, A. Böck, Features of the formate dehydrogenase mRNA necessary for decoding of the UGA codon as selenocysteine, Proceedings of the National Academy of Sciences of the United States of America. 87 (1990) 4660–4664. https://doi.org/10.1073/pnas.87.12.4660.

[48] A.R. Gruber, R. Lorenz, S.H. Bernhart, R. Neuböck, I.L. Hofacker, The Vienna RNA websuite., Nucleic Acids Research. 36 (2008) 70–74. https://doi.org/10.1093/nar/gkn188.

[49] C.J. Wienken, P. Baaske, S. Duhr, D. Braun, Thermophoretic melting curves quantify the conformation and stability of RNA and DNA, Nucleic Acids Research. 39 (2011). https://doi.org/10.1093/nar/gkr035.

[50] V. Moulton, P.P. Gardner, R.F. Pointon, L.K. Creamer, G.B. Jameson, D. Penny, RNA folding argues against a hot-start origin of life, Journal of Molecular Evolution. 51 (2000) 416–421. https://doi.org/10.1007/s002390010104.

[51] L.M.T.R. Lima, J.L. Silva, Positive contribution of hydration on DNA binding by E2c protein from papillomavirus, Journal of Biological Chemistry. 279 (2004) 47968–47974. https://doi.org/10.1074/jbc.M407696200.

[52] J.L. Cole, J.W. Lary, T. P. Moody, T.M. Laue, Analytical Ultracentrifugation: Sedimentation Velocity and Sedimentation Equilibrium, Methods in Cell Biology. 84 (2008) 143–179. https://doi.org/10.1016/S0091-679X(07)84006-4.

[53] P.H. Brown, P. Schuck, Macromolecular size-and-shape distributions by sedimentation velocity analytical ultracentrifugation, Biophysical Journal. 90 (2006) 4651–4661. https://doi.org/10.1529/biophysj.106.081372.

[54] M.C. Micheletto, L.F.S. Mendes, L.G.M. Basso, R.G. Fonseca-Maldonado, A.J. Costa-Filho, Lipid membranes and acyl-CoA esters promote opposing effects on acyl-CoA binding protein structure and stability, International Journal of Biological Macromolecules. 102 (2017) 284–296. https://doi.org/10.1016/j.ijbiomac.2017.03.197.

[55] A. Roy, A. Kucukural, Y. Zhang, I-TASSER: A unified platform for automated protein structure and function prediction, Nature Protocols. 5 (2010) 725–738. https://doi.org/10.1038/nprot.2010.5.

[56] M.R. Wilkins, E. Gasteiger, A. Bairoch, J.C. Sanchez, K.L. Williams, R.D. Appel, D.F. Hochstrasser, Protein identification and analysis tools in the ExPASy server., Methods in Molecular Biology (Clifton, N.J.). 112 (1999) 531–552. https://doi.org/10.1385/1-59259-584-7:531.

[57] M. V. Petoukhov, D. Franke, A. V. Shkumatov, G. Tria, A.G. Kikhney, M. Gajda, C. Gorba, H.D.T. Mertens, P. V. Konarev, D.I. Svergun, New developments in the ATSAS program package for small-angle scattering data analysis, Journal of Applied Crystallography. 45 (2012) 342–350. https://doi.org/10.1107/S0021889812007662.

[58] H. Fischer, M. De Oliveira Neto, H.B. Napolitano, I. Polikarpov, A.F. Craievich, Determination of the molecular weight of proteins in solution from a single small-angle X-ray scattering measurement on a relative scale, Journal of Applied Crystallography. 43 (2010) 101–109. https://doi.org/10.1107/S0021889809043076.

FIGURES

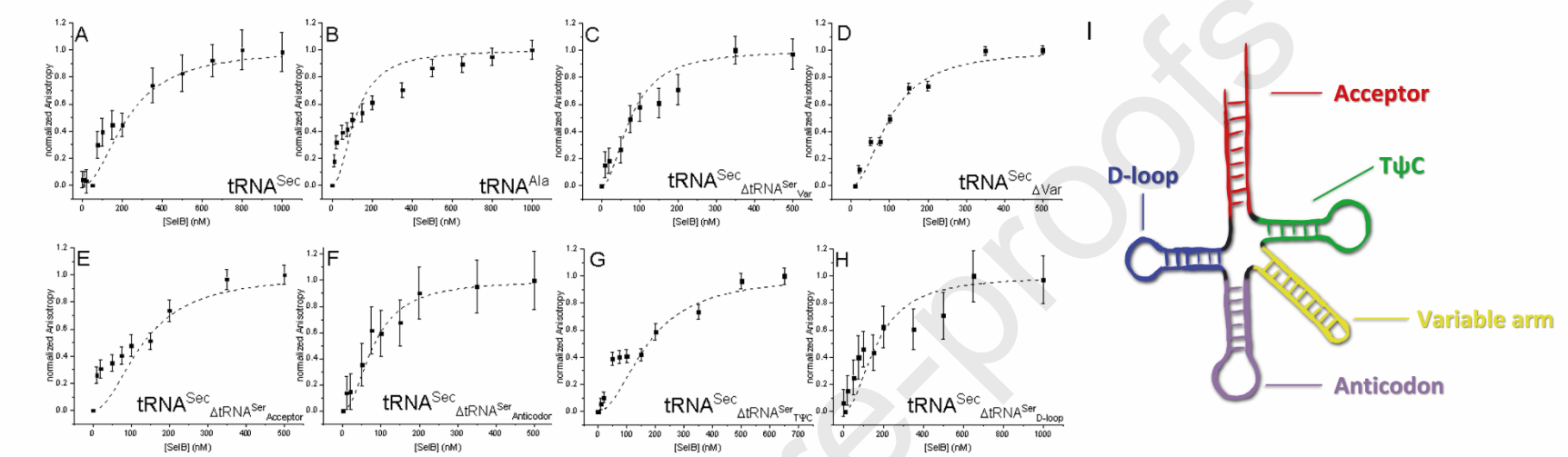

Figure 1: Binding constants of SelB and its tRNA^{Sec} variants. Binding assays performed by fluorescence anisotropy using (A) tRNA^{Sec}; (B) tRNA^{Ala}; (C) tRNA$^{Sec}_{Var}$; (D) tRNA$^{Sec}_{\Delta Var}$; (E) tRNA$^{Sec}_{Acceptor}$; (F) tRNA$^{Sec}_{Anticodon}$; (G) tRNA$^{Sec}_{T\Psi C}$ and (H) tRNA$^{Sec}_{D\text{-}loop}$. (I) tRNA^{Sec} scheme of the mutated regions colored for each specific region. The tRNAs were covalently labeled with fluorescein maleimide with sequentially activated SelB titrations. The obtained dissociation constants by *Hill* adjust (dashed lines) are summarized in **Table 1**. All experiments were performed in biological triplicates and shown in normalized (0-1) anisotropy values.

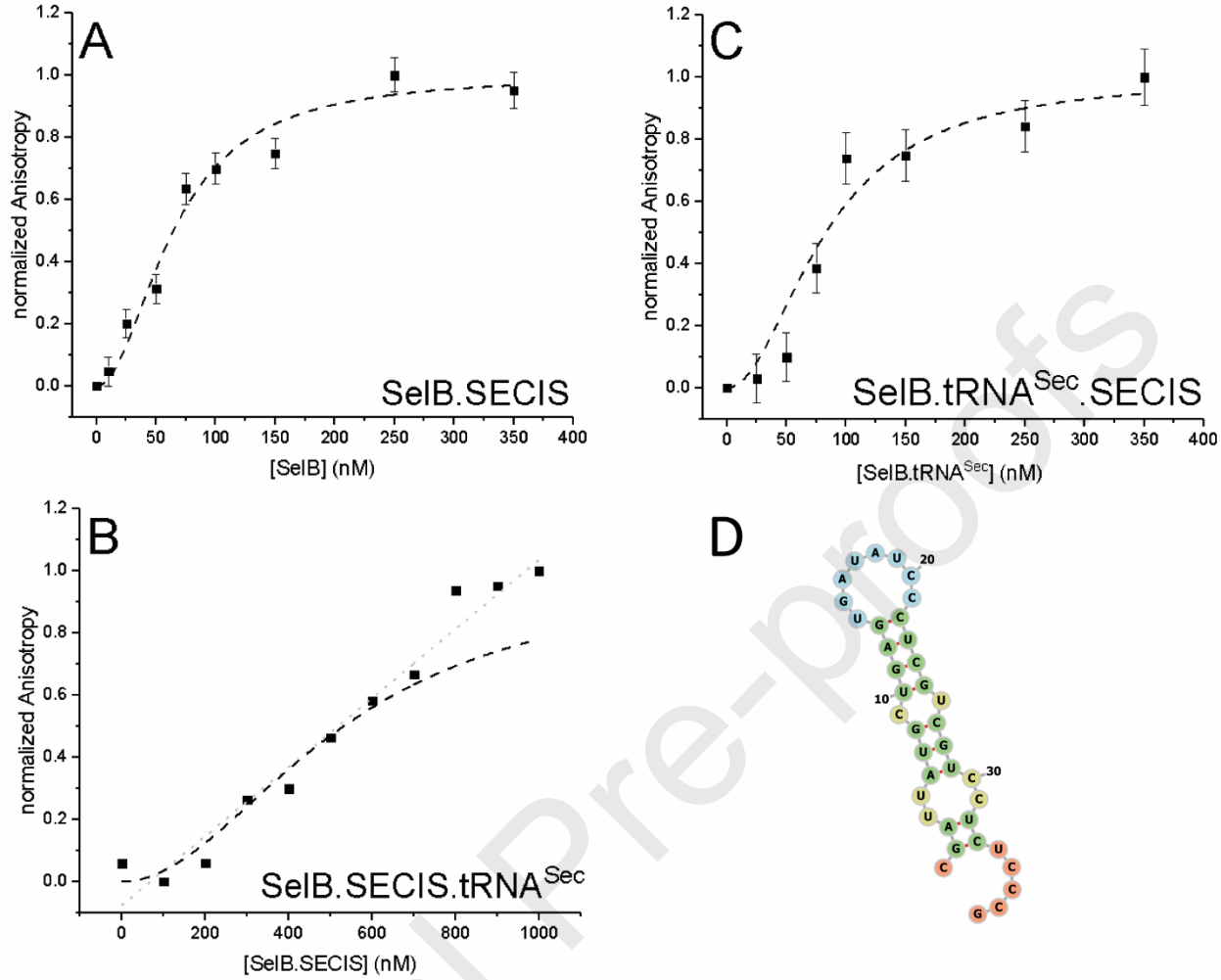

Figure 2: Interaction with Sec pathway partners. Fluorescence anisotropy assays using $tRNA^{Sec}$ and/or SECIS. (A) SelB.SECIS complex formation was evaluated using fluorescein-labeled SECIS with SelB titrations resulting in a specific binding with high affinity. (B) SelB.SECIS complex was titrated against labeled $tRNA^{Sec}$, which resulted in low specificity and almost linear (nonspecific, represented by the straight line in grey) interaction. (C) SelB.$tRNA^{Sec}$ titration against labeled SECIS revealed high affinity and specific binding, suggesting a preferential ordering for complex assembly. The dissociation constants were obtained by *Hill* adjust (dashed lines) and are summarized in **Table 4**. All experiments were performed in biological triplicates and represented in normalized (0-1) anisotropy values. (D) FHD-H SECIS secondary structure prediction using RNAfold web server and colored based on its secondary conformation [48].

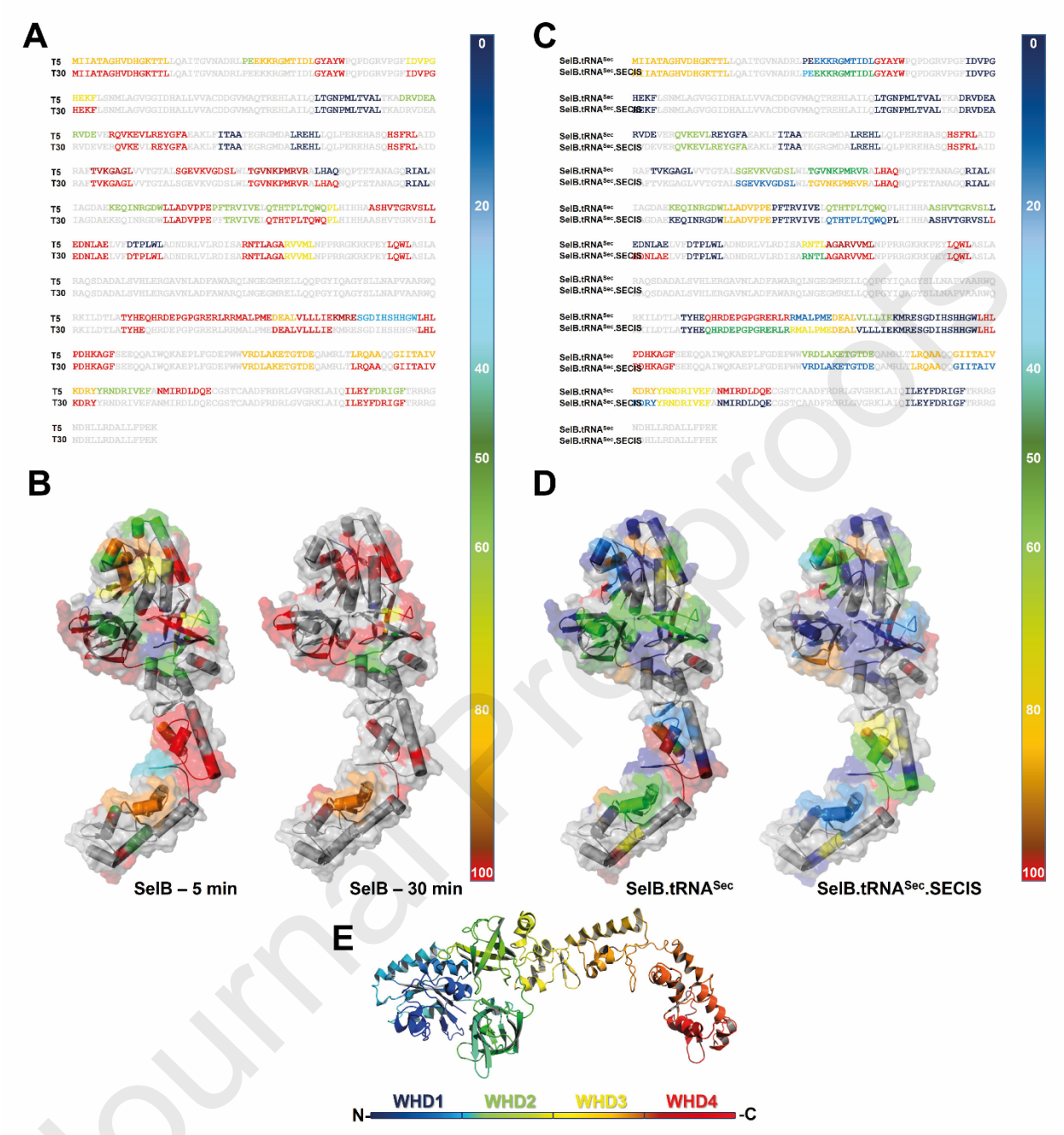

Figure 3: Surface mapping by HDx in complexes formation. (A) Deuterium labeling representation mapped onto the primary structure of SelB at 5 and 30 min. (B) Tridimensional representation of deuterium incorporation using SelB homology model. (C) H/D exchange representation mapped onto the primary structure of SelB at 30 min of deuterium staining in the presence of $tRNA^{Sec}$ and SECIS element and (D) using the SelB homology model. Deuterium incorporation heatmap range: Dark blue to Blue (0-20%); Light blue to Cyan (20-40%); Dark green (50%); Green to Yellow (60-80%) and Orange to Red (80-100%). (E) SelB homology model representing its domain organization and colored in rainbow from N- to C-terminus.

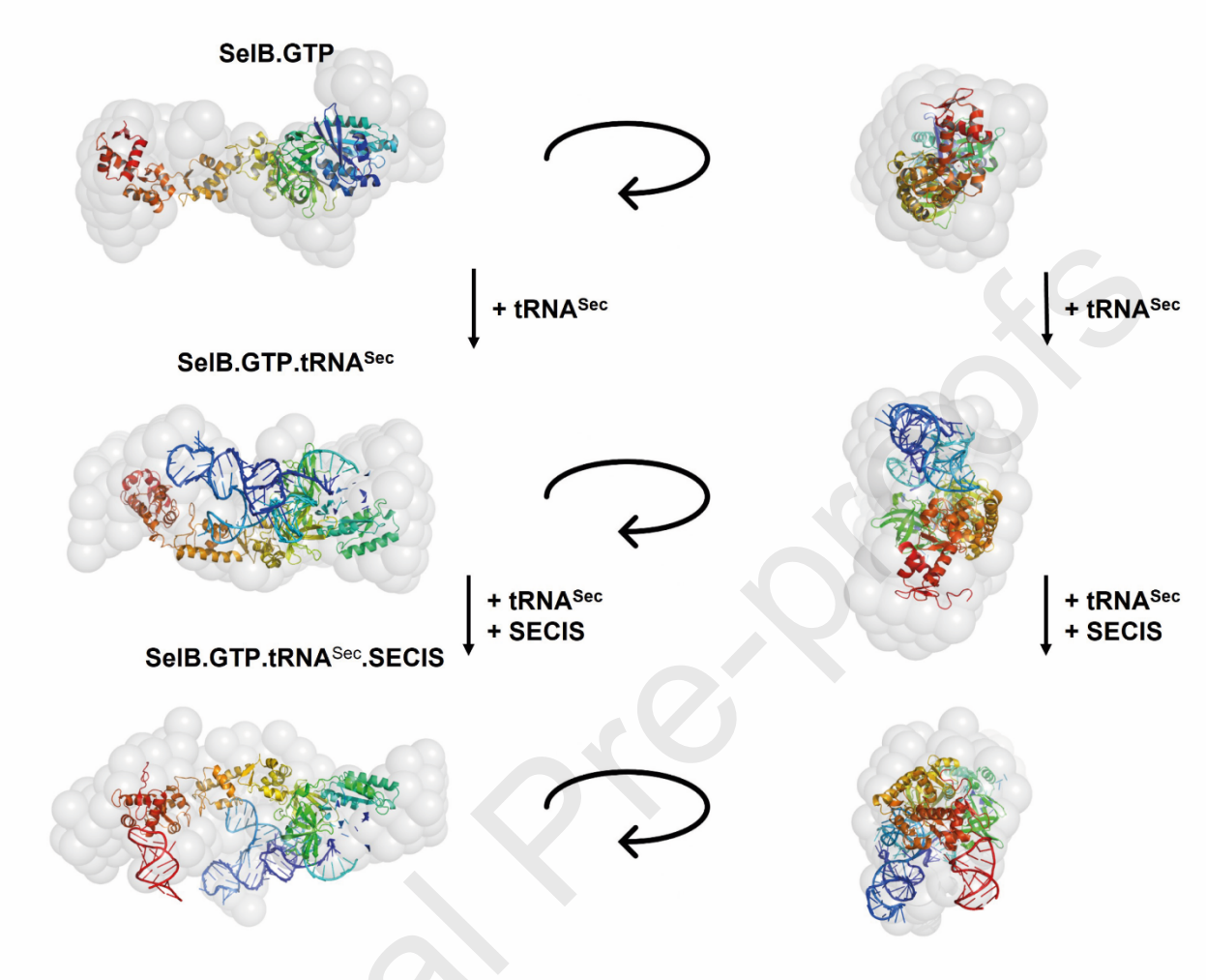

Figure 4: ***In solution*** **molecular envelope of SelB ant its complexes.** Molecular envelope fitted with molecular models obtained by homology modeling of SelB, SelB.tRNA^{Sec}, and SelB.tRNA^{Sec}.SECIS.

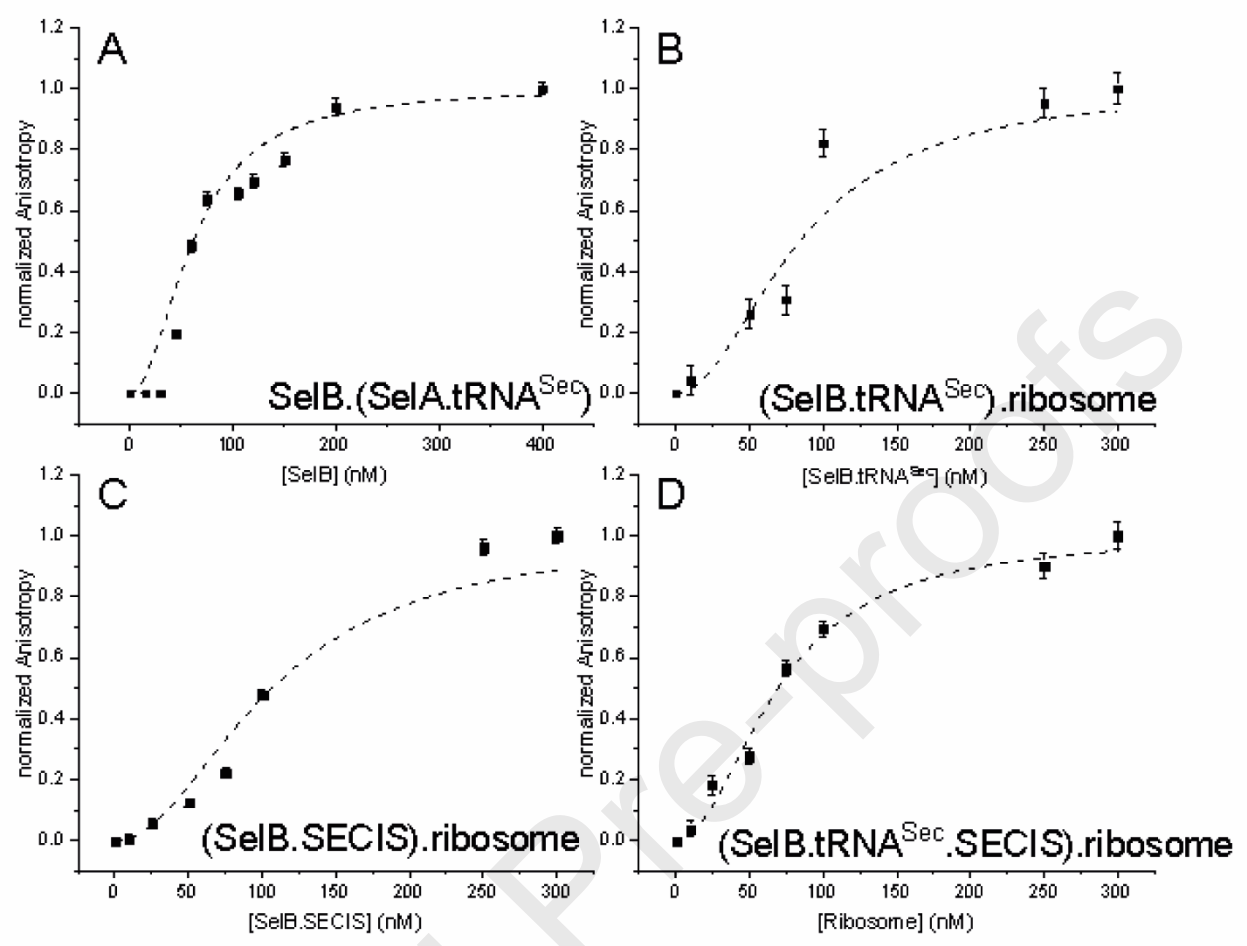

Figure 5: tRNA^{Sec} recognition. The sequential interaction from tRNA^{Sec} maturation to Sec delivery was analyzed using fluorescence anisotropy. (A) Labeled-SelA.tRNA^{Sec} complex against SelB; (B) Labeled-SelB.tRNA^{Sec} complex against ribosome; (C) Labeled-SelB.SECIS complex against ribosome and (D) Labeled-SelB.tRNA^{Sec} in complex with SECIS against ribosome. The dissociation constants obtained by *Hill* adjust (dashed lines) are represented in **Table 4**. As previously demonstrated, the SelA.tRNA^{Sec} binary complex is essential for Ser-Sec conversion. In order to understand SelB specific interaction, fluorescein-labeled tRNA^{Sec} in complex with SelA was previously incubated in 1:1 stoichiometry ration and SelB was titrated, resulting in high-affinity interaction. Posteriorly, tRNA^{Sec} delivery in the ribosome (B-D) showed the preferential interaction pre-assembled SelB.tRNA^{Sec}.SECIS complex. All experiments were performed in biological triplicate and using GTP concentration of 100 mM and the final analysis was shown in normalized (0-1) anisotropy values.

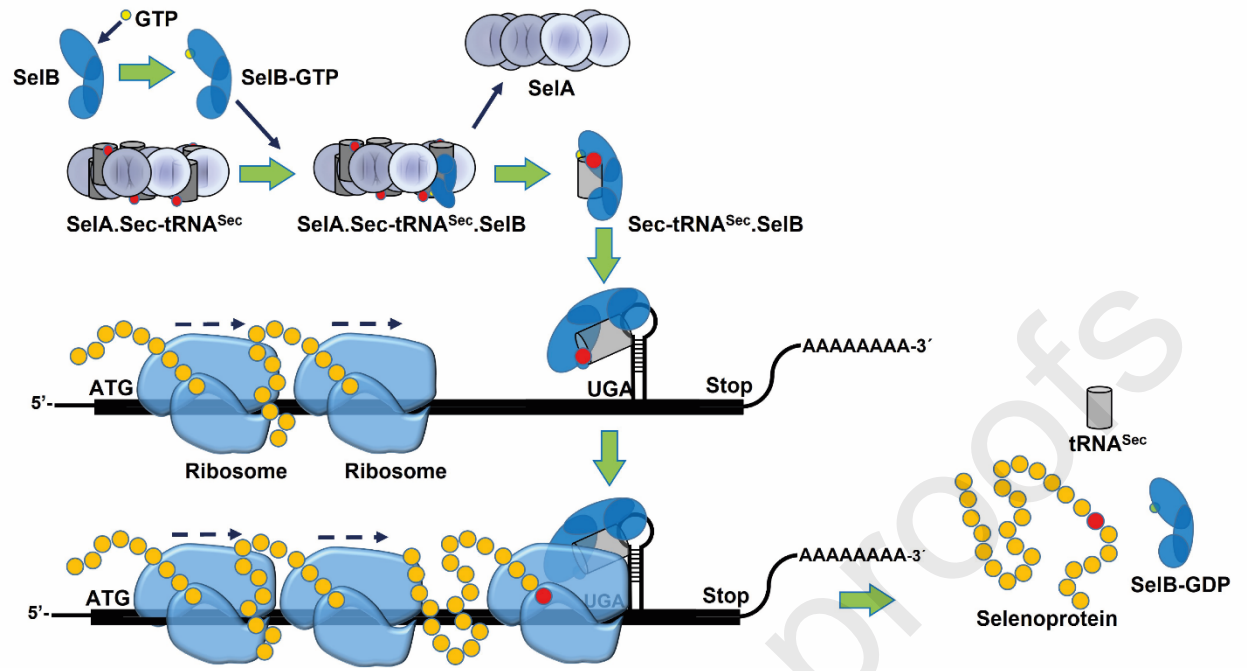

Figure 6: Proposed tRNA^{Sec} incorporation mechanism. Delivery of mature tRNA^{Sec} is initially recognized by SelA and then transferred to the activated SelB.GTP. The SECIS-mRNA further recognition allows the proper deliver the Sec-tRNA^{Sec} to the ribosome for its incorporation into the nascent selenoprotein.

TABLES

Table 1: tRNA^{Sec} specific recognition. Dissociation constants were obtained by fluorescence anisotropy using tRNA^{Sec} variants.

		K_D (nM)	*n*	r^2
Controls	tRNA^{Sec}	283 ± 53	1.4 ± 0.6	0.95
	tRNA^{Ala}	646 ± 129	0.6 ± 0.1	0.91
Deletion	tRNA$^{Sec}_{\Delta Var}$	721 ± 90	1.1 ± 0.2	0.90
ΔtRNA^{Ser}	tRNA$^{Sec}_{Var}$	491 ± 44	1.2 ± 0.1	0.95
	tRNA$^{Sec}_{Acceptor}$	584 ± 89	0.8 ± 0.1	0.91
	tRNA$^{Sec}_{Anticodon}$	269 ± 29	0.9 ± 0.1	0.96
	tRNA$^{Sec}_{T\Psi C}$	501 ± 69	1.0 ± 0.1	0.91
	tRNA$^{Sec}_{D\text{-}loop}$	285 ± 42	0.9 ± 0.1	0.92

K_D, dissociation constant obtained by *Hill* adjust
n, cooperativity (*Hill*) index
r^2, standard deviation from linear adjust

Table 2: Hydrodynamic parameters. SelB interaction and specificity to tRNA^{Sec} structures recognition determined by sedimentation velocity analytical ultracentrifugation.

		***sw* (S)**	***sw*(20,w) (S)**	**MW (kDa)**	**R*s* (nm)**
Control	SelB	4.51	4.78	63.4	3.17
Binding controls	tRNA^{Sec}	6.89	7.31	120.0	3.91
	tRNA^{Ala}	7.56	8.01	137.7	4.10
Deletion	tRNA$^{Sec}_{\Delta Var}$	4.67	4.96	67.0	3.22
ΔtRNA^{Ser}	tRNA$^{Sec}_{Acceptor}$	7.15	7.58	126.7	3.99
	tRNA$^{Sec}_{Anticodon}$	-	-	-	-
	tRNA$^{Sec}_{T\Psi C}$	7.25	7.70	129.5	4.02
	tRNA$^{Sec}_{D\text{-}loop}$	7.67	8.13	140.8	4.13

MW, molecular weight
R_s, *Stoke* (hydrodynamic) radii

Table 3: Dissociation constants obtained by AUC in equilibrium. The obtained K_Ds revealed the affinity of SelB to $tRNA^{Sec}$ variable arm deletion in comparison with $tRNA^{Sec}$ and $tRNA^{Ala}$. K_D's were obtained by the model (A+B → AB)

	SelB molar ratio	K_D (nM)	rmsd
$tRNA^{Sec}$	0.5	230.21	0.02
	1	261.03	0.04
	2	277.93	0.04
		K_{Davg} = 256.4	-
$tRNA^{Ala}$	0.5	610.93	0.03
	1	629.74	0.01
	2	629.92	0.05
		K_{Davg} = 623.5	-
$tRNA^{Sec}_{\Delta Var}$	0.5	794.33	0.02
	1	700.12	0.05
	2	773.19	0.02
		K_{Davg} = 755.9	-

K_D, dissociation constant obtained by *Hill* adjust
K_{Davg}, averaged dissociation constant obtained by individual *Hill* adjust
rmsd, standard deviation from residual

Table 4: SEC pathway affinity constants. Determined K_D and cooperativity index (n) obtained by *Hill* adjustment.

	K_D (nM)	n	r^2
SelB.GTP.$tRNA^{Sec}$	283 ± 53	1.4 ± 0.6	0.99
SelB.GTP.SECIS	57 ± 13	2.6 ± 1.5	0.95
SelB.GTP.SECIS.$tRNA^{Sec}$	895 ± 57	1.8 ± 0.8	0.82
SelB.GTP.$tRNA^{Sec}$.SECIS	77 ± 3	7.3 ± 2.5	0.98
SelB.GTP.SelA.$tRNA^{Sec}$	72 ± 14	2.4 ± 0.9	0.95
SelB.GTP.$tRNA^{Sec}$.ribosome	84 ± 6	7.3 ± 3.2	0.95
SelB.GTP.SECIS.ribosome	110 ± 9	3.3 ± 0.7	0.97
SelB.GTP.SECIS.$tRNA^{Sec}$.ribosome	21 ± 2	2.0 ± 1.0	0.96

K_D, dissociation constant obtained by *Hill* adjust
n, cooperativity (*Hill*) index
r^2, standard deviation from linear adjust

Table 5: Thermodynamics parameters for the unfolding transition of SelB and its complexes.

	T_M (°C)	ΔH_{cal} (kcal/mol)
SelB	47.4 ± 0.2	210 ± 10
SelB.GTP	48.1 ± 0.1	220 ± 20
SelB.tRNA^{Sec}	49.0 ± 0.1	210 ± 10
SelB.GTP.tRNA^{Sec}	48.9 ± 0.1	260 ± 10
SelB.GTP.tRNA$^{Sec}_{T\psi C}$	48.8 ± 0.2	220 ± 10
SelB.GTP.tRNA$^{Sec}_{Anticodon}$	48.7 ± 0.2	220 ± 10
SelB.GTP.tRNA$^{Sec}_{Aceptor}$	46.9 ± 0.3	260 ± 20
SelB.GTP.tRNA$^{Sec}_{D\text{-}loop}$	47.3 ± 0.2	170 ± 10
SelB.GTP.tRNA$^{Sec}_{\Delta Var}$	46.1 ± 0.5	160 ± 10
SelB.GTP.tRNA$^{Sec}_{Var}$	46.2 ± 0.5	180 ± 10
SelB.GTP.tRNA^{Ala}	46.9 ± 0.5	130 ± 10
SelB.GTP.SECIS	48.7 ± 0.1	240 ± 10
SelB.GTP.tRNA^{Sec}.SECIS	48.7 ± 0.2	240 ± 10

T_M, melting temperature
ΔH_{Cal}, enthalpy variation during thermal transition

Table 6: Secondary structure content during complexes formation obtained by FTIR deconvolution.

	Secondary structures	SelB.GTP	SelB.GTP.tRNA^{Sec}	SelB.GTP.tRNA^{Sec}.SECIS
	α-helix (1654 cm^{-1})	16	37	4
Disordered	Turns - (1674 cm^{-1})	16	12	1
	Random coils (1644 cm^{-1})	23	22	11
Strands	$\beta_{\perp}$ (1633 cm^{-1})	30	2	25
	$\beta_{\parallel}$ (1623 cm^{-1})	2	23	1
	$\beta_{\perp}$ (1610 cm^{-1})	1	2	2
	$\beta_{\perp}$ (1690 cm^{-1})	3	2	2

Table 7*: In solution* parameters obtained by SAXS.

	D_{max} (Å)	Gyration radii (Å)
SelB.GTP	140 ± 5	47.00 ± 0.04
SelB.GTP.tRNA^{Sec}	160 ± 5	52.90 ± 0.06
SelB.GTP.tRNA^{Sec}.SECIS	170 ± 5	56.70 ± 0.03

D_{max}, maximum distance [57]

Declaration of interests

☒ The authors declare that they have no known competing financial interests or personal relationships that could have appeared to influence the work reported in this paper.

☒The authors declare the following financial interests/personal relationships which may be considered as potential competing interests:

Vitor Hugo Balasco Serrão

Adriano de Freitas Fernandes

Luis Guilherme Mansor Basso

Jéssica Fernandes Scortecci

Edson Crusca Júnior

Marinônio Lopes Cornélio

Bibiana Monson de Souza

Mário Sérgio Palma

Vitor Hugo Balasco Serrão.: Conceptualization, Data curation, Formal analysis, Investigation, Methodology, Project administration, Roles/Writing - original draft. Adriano de Freitas Fernandes.: Conceptualization, Data curation, Formal analysis, Investigation, Methodology, Roles/Writing - original draft. Luis Guilherme Mansor Basso.: Data curation, Formal analysis, Methodology, Roles/Writing - original draft. Jéssica Fernandes Scortecci.: Data curation, Formal analysis, Methodology, Roles/Writing - original draft. Edson Crusca Júnior.: Data curation, Formal analysis.Marinônio Lopes Cornélio.: Data curation, Formal analysis, Methodology. Bibiana Monson de Souza.: Data curation, Formal analysis, Methodology. Mário Sérgio Palma.:

Methodology, Resources. Mario de Oliveira Neto.: Data curation, Formal analysis, Methodology, Validation, Visualization. Otavio Henrique Thiemann.: Conceptualization, Funding acquisition, Project administration, Resources, Supervision, Validation, Visualization, Roles/Writing - original draft.

HIGHLIGHTS

- Elucidate the Sec incorporation pathway having SelB as checkpoint through the dissociation constant values observed in the formation of complexes with tRNA, SECIS element, SelA, and ribosome;
- Determine the order of events in the withdrawal process of mature $tRNA^{Sec}$ from binary complex SelA.$tRNA^{Sec}$ and delivery to the ribosome;
- Low-resolution mapping of SelB and its complexes with $tRNA^{Sec}$ and SECIS element.